Generalized Design Method of Highly-Varied-Helix End Mills for Suppression of Regenerative Chatter in Peripheral Milling

Takehiro Hayasaka[a], Atsushi Ito[b,*], and Eiji Shamoto[a]

[a] Department of Mechanical Science and Engineering, Graduate School of Engineering, Nagoya University, Furo-cho, Chikusa-ku, Nagoya, 464-8603, Japan

[b] Brother Industries, Ltd., 3-8, Momozono-cho, Mizuho-ku, Nagoya, 467-0855, Japan

Abstract

Peripheral finishing of hardened steel by milling has recently been introduced to the machining field, but often causes severe chatter vibration due to high specific cutting force and low stiffness of slender end mills. It was shown in the previous papers [1-3] that highly-varied-helix end mills were effective for the suppression of regenerative chatter, and a low radial immersion was applied to avoid the effect of mode coupling. Especially for the highly-varied-helix end mills, it was proved experimentally that they were effective across a wide range of cutting conditions, making it possible for cutting with a relatively large axial depth of cut to be carried out and thus realizing a high surface generation rate in peripheral milling of hard materials. However, the milling tests were carried out under just one specific condition, i.e., tool diameter 8 [mm], projection length 36 [mm], and workpiece of 60 HRC hardened steel, etc., and the helix angles of the tool were varied large enough to suppress regenerative chatter but with no quantitative discussion for their determination. In this paper, a generalized design method for varied-helix end mills to suppress regenerative chatter is proposed. Namely a design index $\frac{a_p}{a_\text{lim}}$, in which a_p is the distance between 2 adjacent regenerative effect cancellation lines and a_lim is the asymptotic stability limit in the targeted cutting process, is introduced to design the helix angle difference of a tool, and milling experiments are carried out in several conditions to verify the validity of the proposed index.

Keywords: Chatter; Milling; Varied-helix end mill; Hard materials; Regeneration

1   Introduction

High-efficiency and precision machining needs to be conducted in order for companies to satisfy the demands of the market and survive the harsh competition between others. Therefore, the existing machining methods always need to be targets of improvement in terms of efficiency and preciseness. One example of these improved machining methods is the peripheral finishing of hard material by grinding, i.e. there has recently been a movement of replacing this process by peripheral milling for realization of high-efficiency and precision finishing [1-3]. Since finishing is the targeted process, only cutting with a small radial immersion is needed, and therefore the axial depth of cut can be increased enough so that the efficiency exceeds that of grinding.

However, chatter vibration becomes a conflict to the peripheral milling because of the high specific cutting force and low stiffness of slender end mills. Chatter vibration causes practical problems such as poor machining accuracy, large surface roughness, and short tool life, so there is a necessity to be suppressed.

In peripheral milling, two types of chatter vibration become a problem, which are namely the mode coupling chatter and the regenerative chatter. Since end mills are cylindrical in shape, the vibration modes in the perpendicular directions tend to have close resonant frequencies resulting in these modes to couple together and causes mode coupling chatter. Regenerative chatter occurs due to the regeneration of the previously cut surface causing the fluctuation in the

cutting force. Both types of chatter vibration need to be suppressed successfully in order to realize high-efficiency and precision machining.

A simple method to avoid mode coupling chatter is to set the radial immersion of the end mill small. By doing so, the direction of the uncut chip thickness becomes mainly in the radial depth of cut direction, which as a result breaks the linkage between the two modes.

Concerning with regenerative chatter of the milling process, numerous studies have been conducted throughout the years [4-9], and as a result have leaded to a good understanding of the milling process and well-predicted stability limits. In the course of these studies, variable pitch end mills and variable helix end mills, which are called "varied-helix end mills" in this study, have been utilized to suppress regenerative chatter and their effectiveness have also been studied [10-13]. Moreover, "highly-varied-helix end mills", e.g. helix angles of 45 deg and 40 deg, have been proposed recently [1-3] to increase the robustness of "ordinarily-varied-helix end mills" even more. Since the helix angle difference between the teeth is large, multiple positions where the regenerative effect is cancelled appear along the axial position of the end mill, hence having a wide range for stable cutting in terms of spindle speed and axial depth of cut. However, the highly-varied-helix end mills mentioned in the previous studies were not designed under analytical background, but just so that they have a large enough helix difference that is assumed to have a robust performance. In order to discuss the effects of varied-helix end mills in a quantitative manner and utilize them correctly, a guideline is needed for their designs.

In another perspective, it is often difficult to get full benefit of varied-helix end mills in practical machining environments, because the stable conditions for varied-helix end mills are decentralized like a spider web and their accurate prediction is difficult in practice. For example, it is difficult to accurately measure the specific cutting force coefficients and the dynamic compliance of the vibrating structure especially in the rotating condition, and the chatter frequency often shifts to undesignated values. Chatter suppression utilizing the stable conditions often fails due to these uncertainties. The authors' goal is to get rid of these difficulties and attain robustness for even the worst conditions that a process can take.

In the present paper, a universal design index, namely $\frac{a_p}{a_{\lim}}$, is introduced to design robust varied-helix end mills for chatter-free machining. A threshold value of this design index is also derived theoretically, and the effectiveness of the design index is verified analytically and experimentally.

To begin with, a simplification of the peripheral milling model with small radial immersion is introduced to derive the asymptotic chatter stability limit of the machining process in concern. Next, the effect of small radial immersion on mode coupling chatter is discussed with analytical proof, and the effects of varied-helix end mills are explained by utilization of the regenerative effect cancellation diagram. Then, the proposed design index is discussed in detail with a simple calculation that derives the threshold value. Finally, experiments are conducted to confirm the effectiveness of the proposed design index.

2   Peripheral milling model with small radial immersion and effect of highly-varied-helix end mill

2.1   Asymptotic chatter stability limit $a_{\lim}$ of small radial immersion peripheral milling

The mechanism of the regenerative chatter vibration can be explained as shown in Fig 1. As the mechanical structure vibrates, the relative displacement between the tool and the workpiece oscillates leading to the fluctuation of the uncut chip thickness. This change in the uncut chip thickness causes the dynamic cutting force, hence leading to chatter vibration [14].
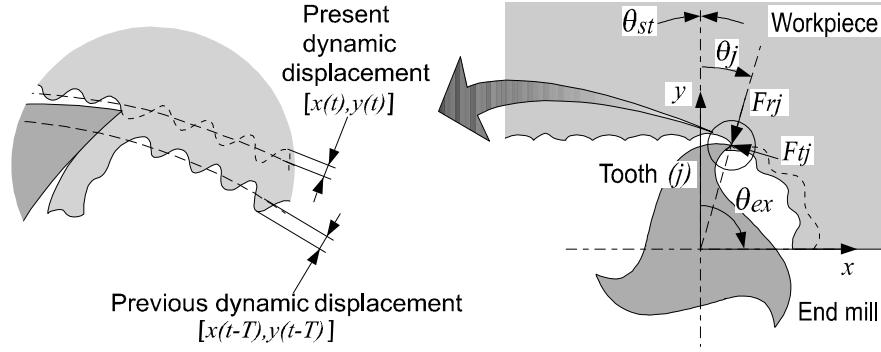
Fig. 1. Peripheral milling model with regenerative chatter vibration.

With the assumption that the end mill is rigid in the axial direction, it is known that the peripheral milling process is ruled by the following equation in which the mode coupling chatter and regenerative chatter are both considered.

$$\begin{Bmatrix} F_x \\ F_y \end{Bmatrix} = \frac{1}{2} a K_t \left(1 - e^{-i\omega_c T}\right) [A][G] \begin{Bmatrix} F_x \\ F_y \end{Bmatrix} \tag{1}$$

Here, F_x and F_y are the dynamic cutting forces in the feed direction and radial depth of cut direction respectively, a is the axial depth of cut, K_t is the tangential specific cutting force, ω_c is the chatter vibration frequency, T is the tooth passing period, $[A]$ is the directional dynamic milling force coefficient matrix, and $[G]$ is the dynamic compliance matrix of the structure in the x and y directions. $[A]$ is given as follows,

$$[A] = \begin{bmatrix} \alpha_{xx} & \alpha_{xy} \\ \alpha_{yx} & \alpha_{yy} \end{bmatrix}$$

$$\alpha_{xx} = \sum_{u=1}^{N_t} -[\sin 2\theta_u + k_r(1 - \cos 2\theta_u)]g(\theta_u)$$

$$\alpha_{xy} = \sum_{u=1}^{N_t} -[(1 + \cos 2\theta_u) + k_r \sin 2\theta_u]g(\theta_u) \tag{2}$$

$$\alpha_{yx} = \sum_{u=1}^{N_t} [(1 - \cos 2\theta_u) - k_r \sin 2\theta_u]g(\theta_u)$$

$$\alpha_{yy} = \sum_{u=1}^{N_t} [\sin 2\theta_u - k_r(1 + \cos 2\theta_u)]g(\theta_u)$$

where N_t is the number of teeth of the end mill, θ_u is the rotational position of tooth u, k_r is the cutting force ratio, i.e. radial specific cutting force is $k_r K_t$, and $g(\theta_u)$ is a unit step function in which its value is 1 if tooth u is during cutting and 0 if not.

In the special case of up or down cut with a small radial immersion, $\theta_u \approx 0$ or π. Hence, a_{xx} and a_{yx} can be approximated as 0, which essentially means that vibration in the feed

direction has no effect on the cutting force. In addition, the cross components G_{xy} and G_{yx} of the dynamic compliance matrix $[G(i\omega_c)]$ are usually small and can be assumed to be equal to 0 here because the end mill is nearly symmetric. Therefore, Eq. (1) can be simplified to the following form.

$$
\begin{Bmatrix} F_x \\ F_y \end{Bmatrix} = \frac{1}{2} aK_t\left(1 - e^{-i\omega_c T}\right) \begin{bmatrix} 0 & \alpha_{xy} \\ 0 & \alpha_{yy} \end{bmatrix} \begin{bmatrix} G_{xx} & 0 \\ 0 & G_{yy} \end{bmatrix} \begin{Bmatrix} F_x \\ F_y \end{Bmatrix}
$$
$$
= \frac{1}{2} aK_t\left(1 - e^{-i\omega_c T}\right) \begin{bmatrix} \alpha_{xy} G_{yy} \\ \alpha_{yy} G_{yy} \end{bmatrix} F_y \tag{3}
$$

Since the dynamic cutting force in the feed direction F_x does not have a closed loop relation, the chatter stability can be evaluated by the following characteristic equation.

$$
1 - \frac{1}{2} aK_t\left(1 - e^{-i\omega_c T}\right)\alpha_{yy} G_{yy} = 0 \tag{4}
$$

Considering the fact that chatter vibration usually occurs at one dominant frequency in many cases, it is well known that the milling force component α_{yy} can be approximated by its average [5] as follows.

$$
\alpha_{yy} \approx \alpha_{0yy} = \frac{N_t}{2\pi} \int_{\theta_{st}}^{\theta_{ex}} (-2k_r)\, d\theta = -2N_t k_r \frac{\theta_{ex} - \theta_{st}}{2\pi} \tag{5}
$$

Here, θ_{st} and θ_{ex} represent the start and exit angles of cutting respectively, and $\frac{\theta_{ex}-\theta_{st}}{2\pi}$ represents the duty ratio of actual immersion time to the entire rotation time and is replaced by r_d.

By separating Eq. (4) into the real and imaginary parts, the asymptotic chatter stability limit a_{lim} can be determined as follows.

$$
a_{lim} = -\frac{1}{N_t r_d} \frac{1}{2k_r K_t G_{yy}^{real}} \tag{6}
$$

Here, G_{yy}^{real} is the negative peak of the real part of the dynamic compliance in the radial depth of cut direction. From Eq. (6), it can be observed that the stability limit in peripheral milling with small radial immersion can be simplified closely to the stability limit of plunge turning which is $b_{lim} = -\frac{1}{2k_r K_t G_{yy}^{real}}$ [14], where b represents the width of cut during plunge turning.

2.2 Relation between small radial immersion and mode coupling chatter

In the ordinary milling process, mode coupling chatter and regenerative chatter both become a crucial problem for efficient machining, and hence are both considered when discussing about chatter stability. Against mode coupling chatter, it is known that it can be neglected when a small radial immersion is applied [1-3]. In fact, it can be observed from Eq. (6) that only the compliance in the radial depth of cut direction G_{yy}^{real} affects the chatter stability limit.

Here, the effect of small radial immersion cutting is observed from a different perspective,

and the critical radial depth of cut, or can be called the critical immersion angle $\theta_{\lim}$ in terms of degree, is calculated analytically. Supposing that the regenerative effect of the milling process is fully cancelled for example by use of varied-helix end mills, i.e. $\Sigma_{u=1}^{N_t}\Sigma_{v=1}^{N_a}e^{-i\omega_c T_{u,v}} = 0$ where N_a is the element number corresponding to the axial depth of cut, the milling process can be expressed by the block diagram shown in Fig. 2.
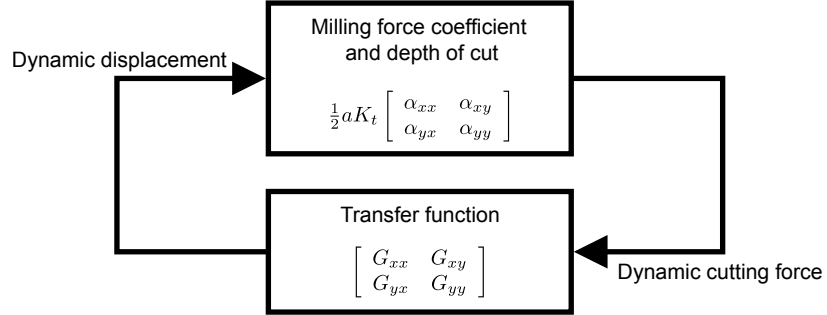

Fig. 2. Block diagram of milling process without regenerative effect.

Using Eq. (1), the following characteristic equation can be derived for this process,

$$\det\left[[I] - \frac{1}{2}a_{\lim}K_t[A_0][G(i\omega_c)]\right] = 0, \ [A_0] = \begin{bmatrix} \alpha_{0xx} & \alpha_{0xy} \\ \alpha_{0yx} & \alpha_{0yy} \end{bmatrix} \tag{7}$$

where $[I]$ is a two dimension identity matrix.

By calculating the stability limit using Eq. (7), the critical immersion angle $\theta_{\lim}$ can be calculated analytically. An example of a simulation result is shown in Fig. 3. The parameters shown in Table 1 are utilized for the simulation.

Table 1
Parameters for simulation

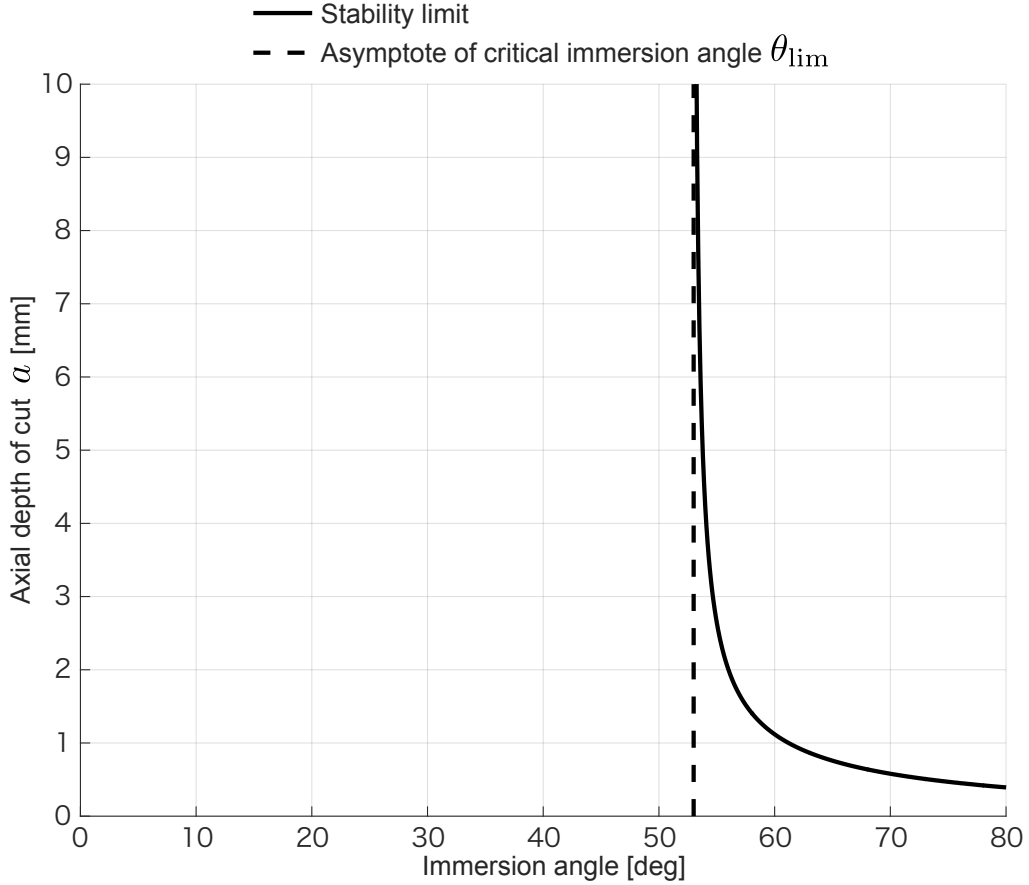|		
Tool geometry	Radius [mm]	4
	Number of teeth N_t	4
	Helix [°]	45/44/45/44
	Axial position of equal pitch [mm]	6.7
Modal parameters m[kg], c[N/(m/s)], k[N/m]		$m_x = 0.0126, \ m_y = 0.0138$ $c_x = 6.62, \ c_y = 5.88$ $k_x = 7.39 \times 10^6, \ k_y = 8.10 \times 10^6$
Cutting direction		Down milling
Specific cutting force	Feed K_t [MPa]	3697.1
	Radial depth of cut K_r [MPa]	2349.9

Fig. 3. Stability limit of milling process for mode coupling.

From the simulation result above, it can be observed that the stability limit increases rapidly as the immersion angle gets smaller and approaches to a certain angle. More precisely, an asymptote to this rapid increase can be derived which is shown as a dashed line in Fig. 3. This asymptote is the critical immersion angle θ_{lim}, and it implies that the mode coupling chatter can be suppressed completely by setting the immersion angle below this critical angle.

2.3 Suppression of regenerative chatter by highly-varied-helix end mill

The effects of the varied-helix end mill have been discussed in the recent years, with them based on the variable pitch end mills [11-13] but acts robustly against the change in spindle speed and chatter frequency. Equation (8) shows the optimal pitch difference between two teeth for suppressing regenerative chatter [3].

$$\frac{60 f_c (\theta_2 - \theta_1)}{n} = (2m + 1)\pi \tag{8}$$

Here, f_c [Hz] is the chatter frequency, θ_1 and θ_2 [rad] are both pitch angles between two teeth, n [min^{-1}] is the spindle speed, and m is an integer number. For simplicity, the negative peak frequency of the real part of the dynamic compliance in the radial depth of cut direction is utilized as f_c, which can be measured by the impulse response method. In the case of a 4-tooth end mill, the pitch angles can have a relation of $\theta_1 = \theta_3$, $\theta_2 = \theta_4$, and $\theta_1 + \theta_2 = \pi$, which is called "alternating pitch variation" [11]. Note that another pitch angle variation called "linear pitch

variation" is also known for robustness against the spindle speed and the chatter frequency. However, this robustness is unnecessary for the proposed design since the purpose of the proposed design is to realize sufficient robustness (against both axial depth of cut and spindle speed below a certain speed) by the large helix angle difference, so only the alternating pitch variation is concerned here.

Equation (8) implies that the difference of two pitch angles between teeth should be set so that the phase difference between the two regenerative vibrations caused by the corresponding teeth should be an odd integer multiple of π [rad]. By doing so, the two vibrations cancel each other out causing no vibration in a comprehensive manner. This can be explained by thinking of the phase delay vector $e^{-i\epsilon_u}$ on the complex plane as shown in Fig. 4, where ϵ_u is the phase delay of a vibration caused by tooth u and $\epsilon_u = \frac{60 f_c \theta_u}{n}$.
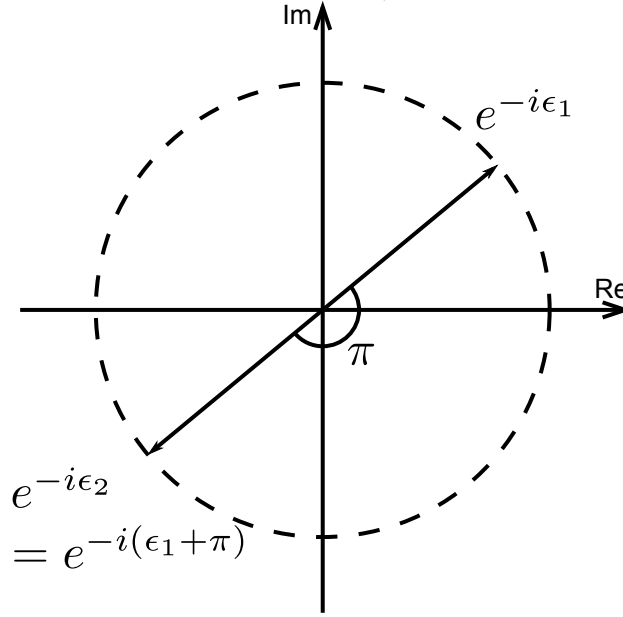

Fig. 4. Relation of phase delay vectors between two regenerative vibrations.

From Eq. (8), the following equation is derived.

$$\epsilon_2 - \epsilon_1 = \frac{60 f_c (\theta_2 - \theta_1)}{n} = (2m + 1)\pi \tag{9}$$

For the case of $m = 0$, the difference between two phase delays becomes π [rad], or in other words $\epsilon_2 = \epsilon_1 + \pi$. From this relation, $e^{-i\epsilon_2} = e^{-i(\epsilon_1 + \pi)}$ is derived, and as a result can be expressed as the two vectors shown in Fig. 4, which makes them cancel each other out and hence stops the vibration from growing.

The cancellation effect of a varied-helix end mill can be explained in a similar manner. In a varied-helix end mill, there is a helix difference between two teeth, which means that the pitch angles between two teeth vary along the height of the end mill. This causes several optimal pitch differences to be placed along the axial direction, whereas the same optimal pitch difference is placed along the axial direction in a variable pitch end mill. Hence, there are several heights where the regenerative vibrations are cancelled out. Now, think of an arbitrary height a_B where the difference of the pitch angles between two teeth is the optimal pitch difference $\varDelta\theta_{\text{opt}}$ [rad], and $\pm\varDelta a$ positions above and below it are described as shown in Fig. 5.
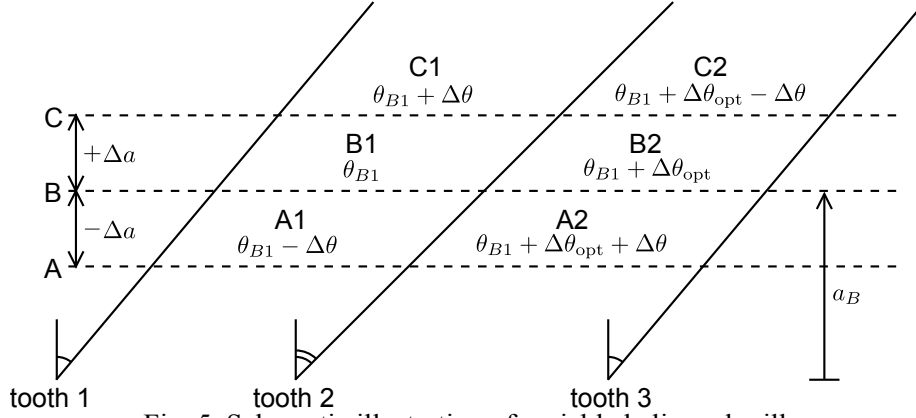
Fig. 5. Schematic illustration of variable helix end mill.

In position A1, where the height is $a_B - \Delta a$, the pitch angle between teeth 1 and 2 is $\theta_{A1} = \theta_{B1} - \Delta\theta$, which means that the phase delay of the vibration is $\epsilon_{A1} = \epsilon_{B1} - \Delta\epsilon$. On the other hand, the pitch angle between teeth 2 and 3 in position C2, where the height is $a_B + \Delta a$, is $\theta_{C2} = \theta_{B1} + \Delta\theta_{\mathrm{opt}} - \Delta\theta$, which means that the phase delay of the vibration is $\epsilon_{C2} = \epsilon_{B1} + \pi - \Delta\epsilon$ ($\because \frac{60 f_c \Delta\theta_{\mathrm{opt}}}{n} = \pi$). This comes to the result that the vibrations caused in positions A1 and C2 cancel each other out since the difference between the phase delays is $\epsilon_{C2} - \epsilon_{A1} = \pi$ as illustrated in Fig. 6, so no regenerative vibration occurs comprehensively. The same cancellation effect happens in positions A2 and C1 in the same manner, which comes to the result that vibrations caused above and below an optimal pitch difference are cancelled out. As a matter of fact, this effect occurs around every height of the optimal pitch difference, which realizes an extreme axial depth of cut without chatter.
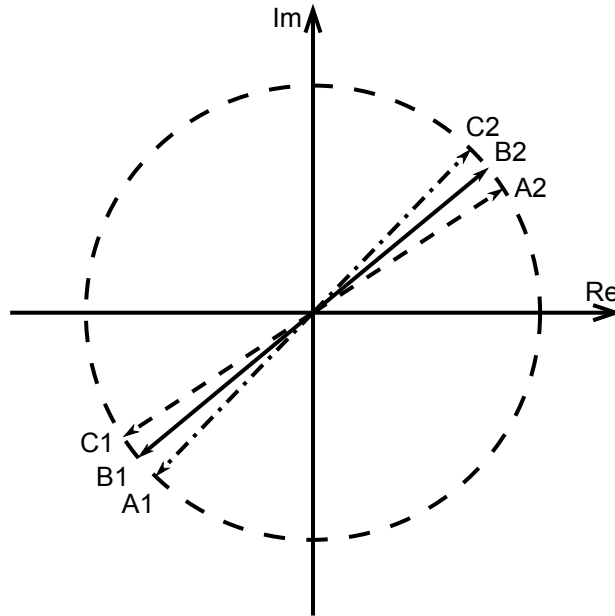

Fig. 6. Cancellation of regenerative vibrations around the height of optimal pitch difference.

This can also be confirmed on the regenerative effect cancellation diagram [3]. An example of a diagram for a varied-helix end mill having a diameter of 8 [mm] with helices of 45 and 44 [deg] is shown in Fig. 7, where the pitch angles between the teeth are equal at the height of 6.7 [mm] from the bottom of the end mill. The dashed lines show the heights of the optimal pitch difference of different m's in Eq. (8), and their heights can be expressed by the following equation.

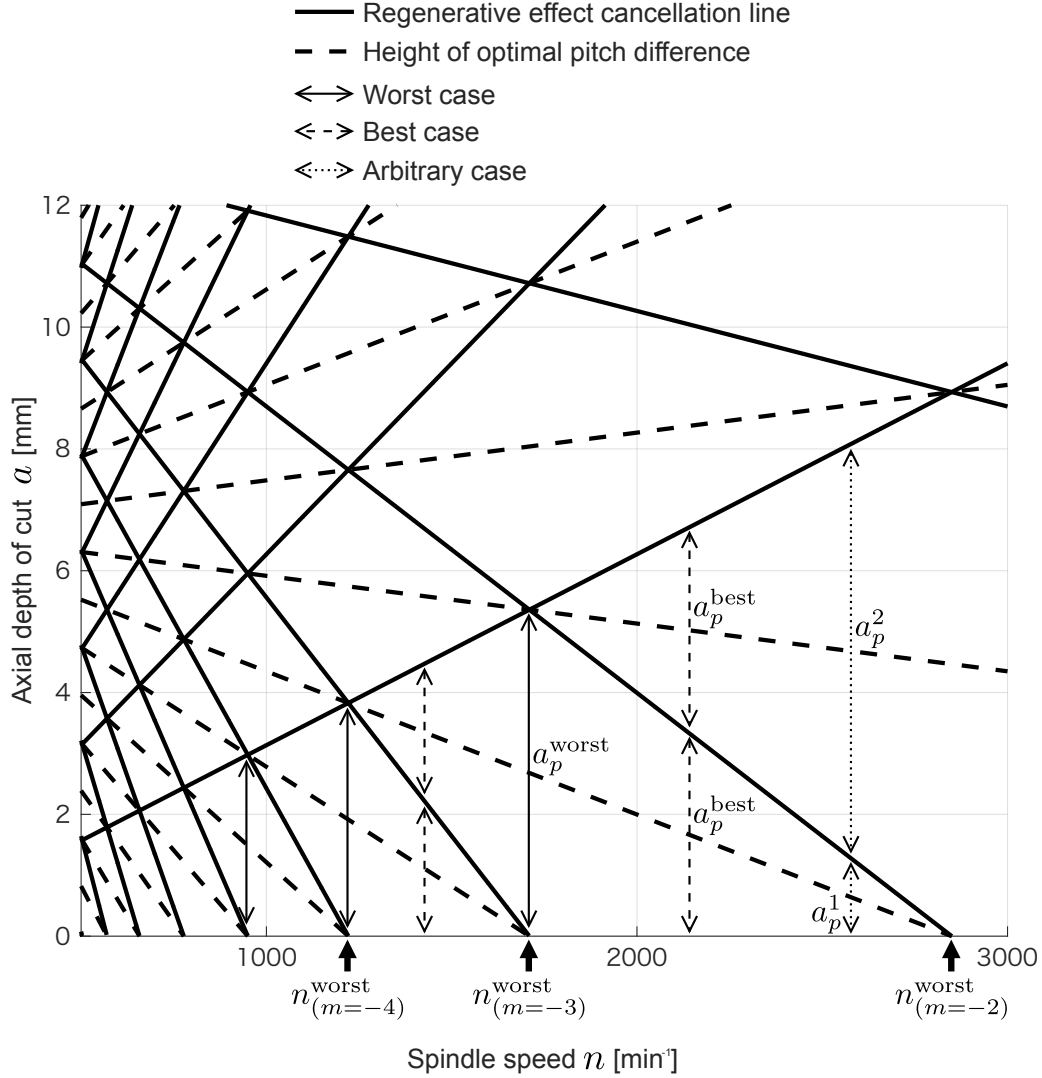$$a_{\mathrm{opt}} = \frac{\pi n D (2m + 1)}{240 f_c |\tan \beta_2 - \tan \beta_1|} + a_{\mathrm{equal}} \tag{10}$$

Fig. 7. Example of regenerative effect cancellation diagram.

Here, a_{opt} is the height of the optimal pitch difference, a_{equal} is the height of equal pitches, and β_1 and β_2 are helices of two alternating teeth. Note that the negative peak frequency of the dynamic compliance in the radial depth of cut direction was utilized for f_c, which is 3894 [Hz] determined from the modal parameters shown in Table 1.

According to the discussion held previously, the regenerative vibrations above and below the optimal pitch difference cancel each other out. Therefore, when cutting is performed at double the height of an arbitrary height of the optimal pitch difference, the vibrations above and below it cancel each other out perfectly and no vibration occurs, or in another perspective cutting at the height of the optimal pitch difference is the worst height since the summation of the regenerative vibrations becomes the maximum at that spindle speed. If the axial depth of cut becomes greater than double the height of the optimal pitch difference, then vibration begins to occur again, and the regenerative effect reaches its maximum at the height of the second optimal pitch difference and again decreases and approaches to 0. These lines where the regenerative effect cancel each

other out are called the "regenerative effect cancellation lines" shown as solid lines in Fig. 7 [3]. The distance from the bottom of the end mill to the height of the regenerative effect cancellation line closest to the bottom of the end mill a_p^1 and the distance between the height of the regenerative effect cancellation line closest to the bottom of the end mill and the next line above it a_p^2 can be expressed as follows.

$$a_p^1 = REM\left(\frac{\pi n D}{120 f_c |\tan\beta_2 - \tan\beta_1|} + 2a_{\text{equal}}, \frac{\pi n D}{60 f_c |\tan\beta_2 - \tan\beta_1|}\right) \tag{11}$$

$$a_p^2 = \frac{\pi n D}{60 f_c |\tan\beta_2 - \tan\beta_1|} - a_p^1 \tag{12}$$

Here, $REM(r, s)$ is a function which returns the remainder of $\frac{r}{s}$.

As can be observed from Eqs. (11) and (12), a_p^1 and a_p^2 take values in the range of $0 \leq (a_p^1, a_p^2) \leq \frac{\pi n D}{60 f_c |\tan\beta_2 - \tan\beta_2|}$. The greater the value, it means that more vibrations of the previous cut surface will regenerate. For the worst case, the distance between the regenerative cancellation lines a_p^{worst} takes a value of $\frac{\pi n D}{60 f_c |\tan\beta_2 - \tan\beta_2|}$, meaning that the process will have the most regenerative vibrations at the height of the optimal pitch difference (shown as solid arrows on Fig. 7) compared to other cases. Note that at a spindle speed of a worst case, i.e. $n_{(m=-2)}^{\text{worst}}$, $n_{(m=-3)}^{\text{worst}}$, or $n_{(m=-4)}^{\text{worst}}$ in Fig. 7, the height of the optimal pitch difference for a specific m value is at the bottom of the end mill. On the other hand, for the best case, $a_p^1 = a_p^2 = a_p^{\text{best}} = \frac{\pi n D}{120 f_c |\tan\beta_2 - \tan\beta_2|}$, which means that the process will have the least regenerative vibrations at the height of the optimal pitch difference compared to other cases (shown as dashed arrows in Fig. 7).

3   Proposal of design index $\dfrac{a_p}{a_{\text{lim}}}$ and its threshold value

The following index for designs of varied-helix end mills is proposed with a_p as the distance between regenerative effect cancellation lines.

Design index for varied-helix end mills : $\dfrac{a_p}{a_{\text{lim}}}$ $\hspace{3cm}$ (13)

This design index has a characteristic that as the value of it becomes smaller, the end milling process becomes more stable against regenerative chatter. For example, if the helix difference between the teeth of an end mill is designed to be large, then a_p becomes small ($\because$Eqs. (11) and (12)) and as a result the value of the design index becomes small. Or in another perspective, if the end mill is designed to be more rigid, then that will lead to small dynamic compliance and hence makes the value of a_{lim} become large ($\because$Eq. (6)), which leads to the value of the design index to be small. Overall, it can be concluded that the design index expressed in Eq. (13) is a generalized index considering the design of helices, the dynamic stiffness of end mills, and even the cutting conditions and workpiece. Note that a_p is considered here as $a_p = a_p^{\text{worst}}$, meaning that the worst case is considered here.

Moreover, the threshold value for the proposed design index can be calculated theoretically for chatter-free milling. In milling with a standard end mill, the regenerative effect is $e^{-i\omega_c T}$ as

shown in Eq. (1) making its absolute value $\left|e^{-i\omega_c T}\right| = 1$, which means that 100% of the vibration on the previously cut surface affects the present cutting process. This percentage can be decreased when using varied-helix end mills. As mentioned in Section 2.3, the summation of the regenerative effect reaches its maximum at the height of the optimal pitch difference. The average value of the summation of the regenerative effect from the bottom of the end mill to the height of the optimal pitch difference can be expressed as follows.

$$\frac{\left|\Sigma_{u=1}^{N_t}\Sigma_{v=1}^{N_{a_p/2}} e^{-i\omega_c T_{u,v}}\right|}{N_t N_{a_p/2}} \tag{14}$$

Here, $N_{a_p/2}$ is the element number corresponding to the height of the optimal pitch difference, and since the time delay of the vibration differs among the teeth and also among the heights, it is expressed as $T_{u,v}$.

Considering the phase delay vectors for the regenerative vibrations caused by a pair of teeth plotted for example in Fig. 6, it is obvious that the following transformation can be performed. In the worst case where the height of optimal pitch difference begins at the bottom of the end mill, the phase delays of the regenerative vibrations caused by the pair of teeth at this height are $\epsilon' \pm \frac{\pi}{2}$. Focusing on the vibrations caused at heights above this height, the phase delay by one tooth gradually increases from $\epsilon' - \frac{\pi}{2}$, and the one for the other tooth gradually decreases from $\epsilon' + \frac{\pi}{2}$. Finally, the phase delays reach $\epsilon' \mp \frac{\pi}{2}$ at the height of the next optimal pitch difference, which is the height with the maximum summation of the regenerative effects. The denominator is 2π when taking the average in the following equation because it includes the effects of both teeth. Note that this explanation is only for the height between $m = 0$ and $m = 1$ in Eq. (9), but it can easily be understood that the same result is obtained for other m values.

$$\frac{\left|\Sigma_{v=1}^{N_{a_p/2}}\left(e^{-i\omega_c T_{1,v}} + e^{-i\omega_c T_{2,v}}\right)\right|}{2N_{a_p/2}} = \frac{\left|\int_{\epsilon'-\frac{\pi}{2}}^{\epsilon'+\frac{\pi}{2}} e^{i\epsilon} d\epsilon + \int_{\epsilon'+\frac{\pi}{2}}^{\epsilon'-\frac{\pi}{2}} e^{-i\epsilon} d\epsilon\right|}{2\pi}$$

$$= \frac{2 \times \left|2e^{i\epsilon'}\right|}{2\pi}$$

$$= \frac{2}{\pi} \tag{15}$$

Although there are $\frac{N_t}{2}$ pairs of teeth that cancel each other out, the value for all the teeth obtained by substituting Eq. (15) into Eq. (14) is the same as above since each pair has the same average value.

$$\frac{\left|\Sigma_{u=1}^{N_t}\Sigma_{v=1}^{N_{a_p/2}}e^{-i\omega_c T_{u,v}}\right|}{N_t N_{a_p/2}}$$

$$= \left(\frac{\left|\Sigma_{v=1}^{N_{a_p/2}}\left(e^{-i\omega_c T_{1,v}} + e^{-i\omega_c T_{2,v}}\right)\right|}{N_{a_p/2}} + \cdots + \frac{\left|\Sigma_{v=1}^{N_{a_p/2}}\left(e^{-i\omega_c T_{N_t-1,v}} + e^{-i\omega_c T_{N_t,v}}\right)\right|}{N_{a_p/2}}\right)/N_t$$

$$= \left(\frac{N_t}{2} \times \frac{4}{\pi}\right)/N_t$$

$$= \frac{2}{\pi} \tag{16}$$

From this equation, we gain the information that $\left(\frac{2}{\pi}\times100\right)\%$ of the regenerative vibration on the previously cut surface affects the present cutting process at the height of the optimal pitch difference when using a varied-helix end mill. More precisely the summation of the percentage of the regeneration of the previous vibration increases from the bottom of the end mill and reaches its maximum at the height of the optimal pitch difference. As a result, the average percentage is equal to $\left(\frac{2}{\pi}\times100\right)\%$.

By multiplying the height from the regeneration effect cancellation line, which is at most $\frac{a_p}{2}$ in any axial depth of cut, by the percentage of the vibration that has the regenerative effect, the equivalent axial depth of cut that affects the present cutting process is obtained. This equivalent depth is in other words the gain of the regenerative cutting process, and by comparing those of cutting using standard end mill and varied-helix end mill, the threshold value of the proposed design index is obtained as follows.

$$\left(\frac{2}{\pi}\times100\right)\% \times \frac{a_p}{2} < 100\% \times a_{\text{lim}} \tag{17}$$

$$\therefore \frac{a_p}{a_{\text{lim}}} < \pi \tag{18}$$

Equation (17) is formulated from the fact that as long as the worst height gain of the regenerative cutting process using the varied-helix end mill does not exceed the limit gain, which is the gain of the regenerative cutting process using the standard end mill, the process is stable. From Eq. (18), it is concluded that as long as the value of the proposed design index is under π, then the cutting process is stable and therefore chatter-free. It should be noted that this equation is derived for the worst height, and thus as long as this equation is satisfied at an arbitrary spindle speed the process is stable at an arbitrary axial depth of cut. Furthermore, the worst case, or $a_p = a_p^{\text{worst}}$, is considered here. This implies that even if a shift occurs in the chatter frequency in the actual cutting process, which means the shift of the best, worst, and arbitrary cases to close spindle speeds, the process is stable as long as Eq. (18) is satisfied since it is the threshold value for the worst case, which is literally the "worst" case an arbitrary spindle speed can take. Note that the shift of the chatter frequency is usually an upward shift, hence meaning that the distance between cancellation lines become closer from Eq. (11). Moreover, considering the worst condition will attain robustness against changes in other parameters such as the specific cutting force and the dynamic compliance, therefore making the proposed design method practical.

From the fact that the percentage calculated in Eq. (18) does not depend on the type of end mill or workpiece, e.g. diameter, dynamic compliance, specific cutting force, helix angles, etc., it can be implied that the proposed design index and its threshold value is a universal one that can be applied to any type of cutting process. Note that only the regenerative vibrations are considered

in Eq. (17), but in the actual cutting process the present vibration also affects the stability of the process. However, even if the present vibration is considered, the process is more stable than just considering the regenerative vibration, so as long as the threshold value is satisfied then the process will always be stable. Note that the distance of the regenerative effect cancellation lines closest to the bottom of the end mill are the most dangerous ones because the effect of the present cutting process is relatively larger than the regenerative cutting process as the axial depth becomes larger, making the cutting more stable.

The validity of Eq. (18) is confirmed by a stability limit simulation using the zero-order solution. Figure 8 shows the stability limit of peripheral milling using a varied-helix end mill, where the dots represent the stability limits and the solid lines represent the regenerative effect cancellation lines. The spindle speed n is taken as the horizontal axis, and the area inside the dots represent unstable regions [15]. The same parameters shown in Table 1 are used for the simulation with an addition of radial depth of cut as 0.0012 [mm], meaning that $r_d = 1.28$ [%].
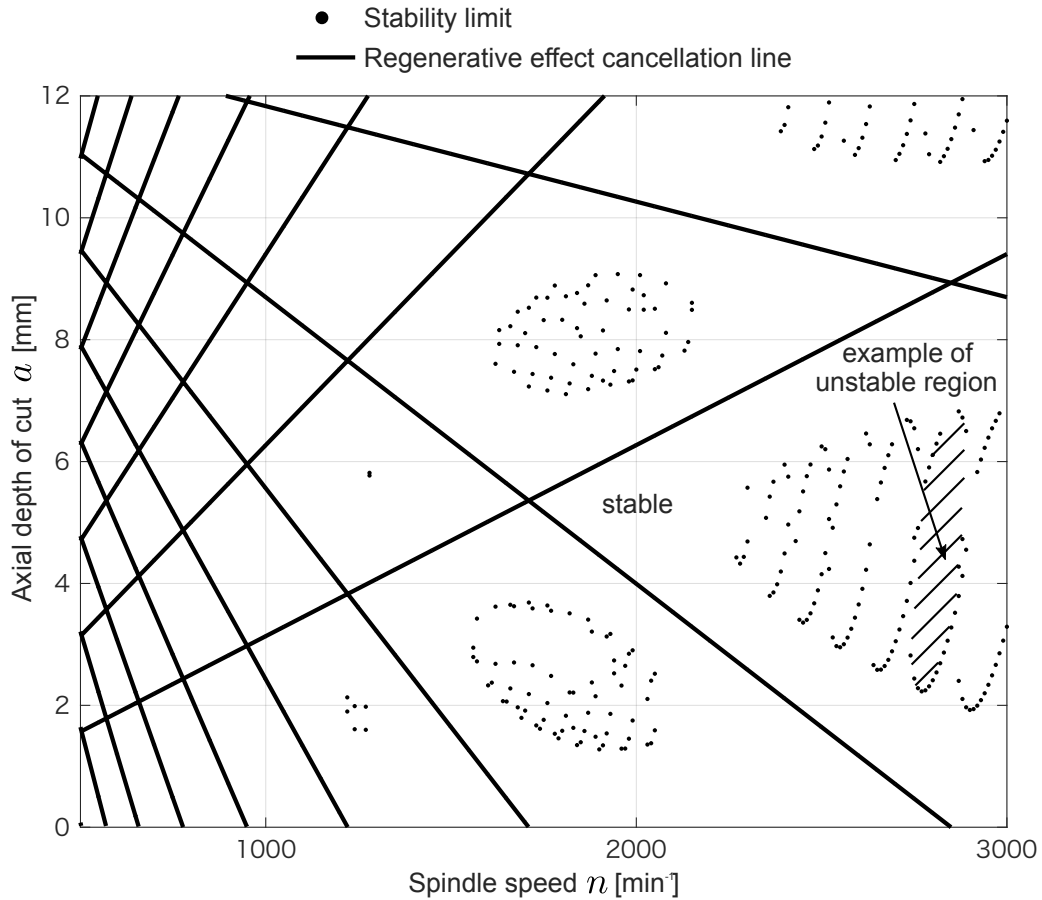
Fig. 8. Relation between regenerative effect cancellation line and stability limit

For simplification, the worst cases are considered here for explanation of the graph. The spindle speeds for the worst cases can be calculated by Eqs. (11) and (12), for example $n = 950, 1221, 1710$ [min⁻¹]. The values of $\frac{a_p}{a_{\text{lim}}}$ for these spindle speeds are $\frac{a_p}{a_{\text{lim}}} = 2.48, 3.19, 4.47$ with $a_{\text{lim}} = 1.20$ [mm] calculated from Eq. (6) using the parameters in Table 1. As can be seen from these values, only the first one satisfies $\frac{a_p}{a_{\text{lim}}} < \pi$. This is why there are no unstable islands at the spindle speed of 950 [min⁻¹] but there are unstable conditions in spindle speeds greater than this. As a result, it can be concluded that a cutting process can be performed chatter-free regardless of the axial depth of cut as long as the milling process is designed so that the proposed design index satisfies Eq. (18).

It has to be mentioned that a best case can be designed intentionally where $a_p^1 = a_p^2 = a_p^{\text{best}}$ for all spindle speeds, meaning that the cutting process is robust even if the chatter frequency shifts from the targeted value. This case can be designed easily by for example setting the height of equal pitches at the bottom of the end mill. In this design, the best case will be maintained for the cutting process even if the chatter frequency shifts, and thus the most robust cutting against chatter vibration can be realized. However, it has to be noted that the chip pocket will be narrow by setting the height of equal pitches at the bottom of the end mill and varying the helix angles large, so these conditions have to be considered in addition for utilization in the real world.

4 Chatter stability experiments and discussions

A series of experiments are carried out to verify the effectiveness of the proposed design index.

4.1 Experimental setup and conditions

A photograph of the experimental setup of the peripheral milling experiment is shown in Fig. 9. A vertical type machining center (MILLAC415V; Okuma Corp.) was employed for the experiment, and a shrink fit holder was used for the tool. The cutting conditions are shown in Table 2. Here, the radial depth of cut, or the immersion angle, was selected according to the simulation shown in Section 2.2 so that mode coupling chatter does not occur. More precisely, a radial depth of cut of 0.012 [mm] (4.618 [°] in immersion angle considering the surface cut by the previous tooth with a feed per tooth $c = 0.025$ [mm/tooth]) was selected, which is extremely small compared to the critical immersion angle shown in Fig. 3.

Table 2
Conditions of cutting experiments

| Tool geometry	Radius [mm]	4	
	Number of teeth N_t	4	
Workpiece		SK105 (60 HRC)	S50C (15 HRC)
Cutting direction		Down milling	
Radial depth of cut [mm]		0.012	
Feed rate [mm/tooth]		0.025	
Maximum uncut chip thickness [mm]		0.002	
Axial depth of cut [mm]		0.5 – 12.5	
Spindle speed [min^{-1}]		2500 – 7000	
Cutting speed [m/min]		63 – 176	
Projection length [mm]		36	41
Tool holder		Shrink holder BT40-SLRB8-75 MST Corp.	
Coolant		Oil mist LB-1 Fuji BC Engineering Co., Ltd.	
Pre-machining condition		Same as shown in this table	
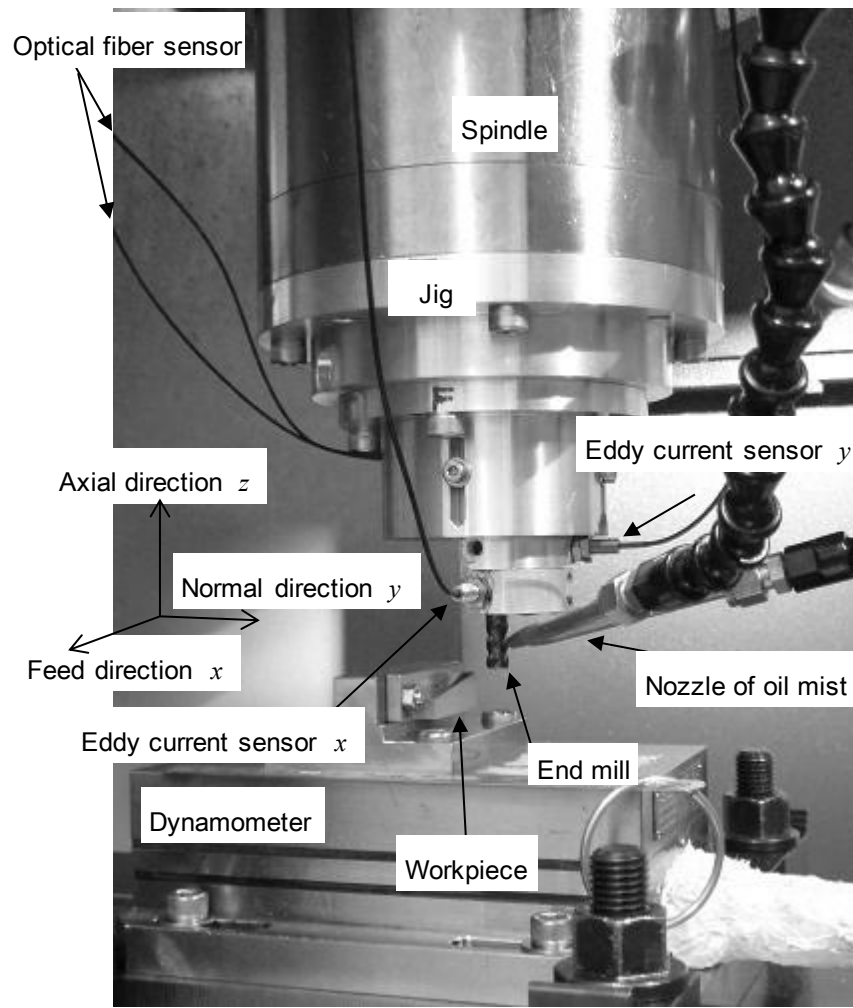
Fig. 9. Setup of peripheral milling experiment.

Measurements were performed on a specially-made jig which was mounted on the spindle housing. Two eddy current displacement sensors (AEC-5706PS; Applied Electronics Corp.) were fixed to the jig to measure displacements of the end mill in the feed (x) and radial depth of cut (y) directions during machining. An optical sensor (FS-V31M; Keyence Corp.) was also fixed to the jig in order to measure the spindle speed accurately.

4.2 End mills and workpieces

Three types of end mills were tested to verify the effectiveness of the proposed design index. Their specifications are shown in Table 3. One is a standard 4-tooth end mill with constant pitch and helix angles (WXS-EMS No.3041080; OSG Corp.). Another is an ordinarily-varied-helix end mill with helix angles of 45 deg/44 deg, and the last one is a highly-varied-helix end mill with helix angles of 45 deg/40 deg. The large helix angle difference means that the pitch angles vary significantly along the axial position of the end mill, thus resulting in high robustness against regenerative chatter.

Table 3
Specifications of tested end mills

No.	Type	Number of teeth	Helix angle [°]	Pitch angle [°]
1	Standard	4	45.0	90.0
2	Ordinarily-varied-helix	4	45.0/44.0/45.0/44.0	Equal pitch at 7.7 [mm] from tip
3	Highly-varied-helix	4	45.0/40.0/45.0/40.0	Equal pitch at 7.7 [mm] from tip

Two workpieces shown in Fig. 10 are prepared for the experiment, with the smaller one having a width of 0.5 to 6.5 [mm], and the larger one having 6.5 to 12.5 [mm]. The workpiece materials utilized were 15 HRC annealed steel (ISO S50C) and 60 HRC hardened steel (ISO C105U). Figure 11 shows the axial setting between the end mill and the workpiece. The bottom of the workpiece is set at a height of 1 [mm] from the bottom of the end mill, and the workpiece is cut continuously to gain multiple information with the assumption that the cutting processes at each height do not interfere with each other.
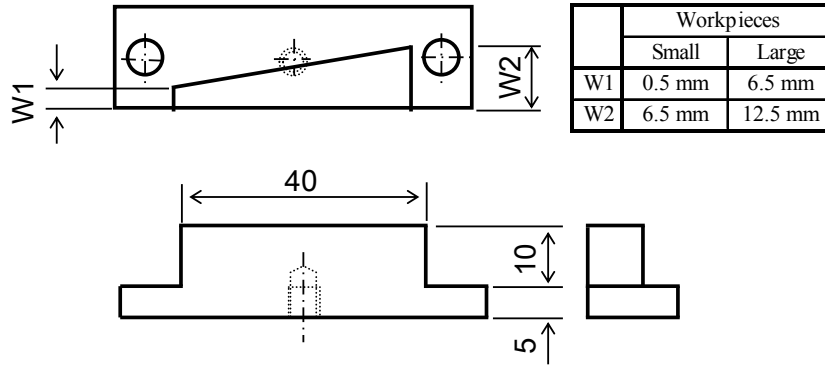
Fig. 10. Workpieces for cutting experiments.
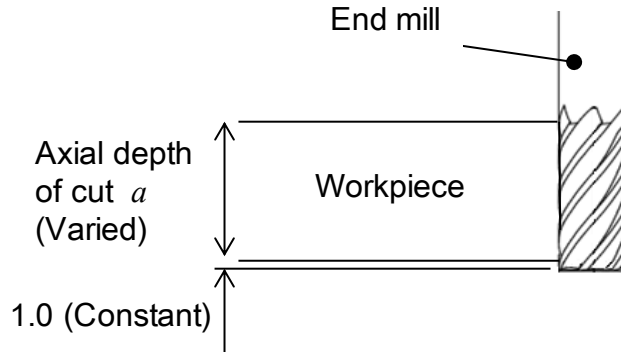
Fig. 11. Axial setting of tool and workpiece.

The calculation of the proposed design index for the two varied-helix end mills are shown in Table 4. Note that a_p^{worst} is calculated for all spindle speeds and used for evaluation with the idea that as long as Eq. (18) is satisfied for the worst case, the cutting process is stable. The values for three different conditions, namely projection lengths of 36, 41, and 46 [mm], for each end mill are calculated. a_{lim} is calculated by Eq. (6) and Table 1 with the number of teeth $N_t = 4$, duty ratio compared to plunge turning $r_d = 1.28$ [%], specific cutting force in the radial depth of cut direction for 60 HRC hardened steel $k_r K_t = 2349.9$ [MPa] (measured in a special turning

experiment shown in [2]), and the negative peak of the real part of the dynamic compliance in the radial depth of cut direction for each end mill (calculated by using the 3rd row in Table 4 and the value G_{yy}^{real} for the end mill set at projection length of 36 [mm]) utilized. Note that despite the fact that cutting is performed in an extremely small radial immersion where the nose edge radius and size effect have a great influence, the specific cutting force is confirmed as a constant value. The specific cutting force for 15 HRC annealed steel is calculated by using the measured ratio compared with milling 60 HRC steel (5th row in Table 4), and the negative-peak frequency for each end mill is utilized as f_c.

Table 4
Calculation of a_p/a_{lim}

Projection length [mm]		36		41		46
Negative-peak frequency [Hz]		3906		3437		2627
Compliance ratio compared with 36 [mm] projection length		1		1.36		2.56
Hardness of workpiece [HRC]		60		15		15
Ratio of normal cutting force compared with milling 60 HRC steel		1		0.573		0.573
a_{lim} [mm]		1.41		1.81		0.96
Helix angle $\beta_2 = 45°$, $\beta_1 = 40°$ n [min^{-1}]	a_p [mm]	a_p/a_{lim}	a_p [mm]	a_p/a_{lim}	a_p [mm]	a_p/a_{lim}
7000	4.67	3.31	5.30	2.93	6.94	7.21
6000	4.00	2.84	4.54	2.51	5.95	6.18
5000	3.33	2.36	3.79	2.09	4.95	5.15
4000	2.67	1.89	3.03	1.68	3.96	4.12
3000	2.00	1.42	2.27	1.26	2.97	3.09
2500	1.67	1.18	1.89	1.05	2.48	2.57
Helix angle $\beta_2 = 45°$, $\beta_1 = 44°$ n [min^{-1}]	a_p [mm]	a_p/a_{lim}	a_p [mm]	a_p/a_{lim}	a_p [mm]	a_p/a_{lim}
7000	21.88	15.52	24.86	13.75	32.53	33.81
6000	18.75	13.30	21.31	11.79	27.88	28.98
5000	15.63	11.08	17.76	9.82	23.24	24.15
4000	12.50	8.87	14.21	7.86	18.59	19.32
3000	9.38	6.65	10.66	5.89	13.94	14.49
2500	7.81	5.54	8.88	4.91	11.62	12.07

As can be observed from the table, the value of the proposed design index of the highly-varied-helix end mill is smaller than the threshold value π in most of the conditions for the projection length of 36 [mm] (with the exception for spindle speed of 7000 [min^{-1}]), in all of the conditions for the projection length of 41 [mm], and in only some conditions, namely conditions of spindle speed of 2500 and 3000 [min^{-1}], for the projection length of 46 [mm]. On the other hand, the one for the ordinarily-varied-helix end mill is larger than the threshold value for all conditions. From these observations, it can be predicted that the highly-varied-helix end mill is stable in almost all conditions of 36 and 41 [mm], and somewhat stable for the projection length of 46 [mm], while the ordinarily-varied-helix end mill is unstable in cutting conditions away from the regenerative effect cancellation lines since the values of the proposed design index at those heights do not satisfy Eq. (18). Since these values are calculated for the worst case, the evaluated stabilities will be valid against practical shifts of stable conditions due to deviation of utilized parameters, e.g. shift of chatter frequency, change of specific cutting force, change of dynamic compliance, etc.

4.3   Measurement of dynamic compliance of end mill by impulse response method

The dynamic compliance of the end mill in the radial depth of cut direction at the tool tip was measured by the impulse response method before each experiment. Those of the tool set at the projection length of 36, 41, and 46 [mm] were measured using a miniature hammer (086D80; PCB Piezotronics Inc.). A fiber optical displacement sensor (ST-3711; Iwatsu Electric Co., Ltd.) was fixed on the machine table to measure the vibration in the radial depth of cut direction.

Figures 12, 13, and 14 show some examples of the results of the dynamic compliances of the tool. Figure 12 shows the dynamic compliance of a 4-tooth standard end mill (No. 1) set at the projection length of 36 [mm] in both the feed and radial depth of cut directions respectively. G^{real} and G^{imag} are the real and imaginary parts of the dynamic compliances. As shown in Fig. 12(a), the negative peak frequency at which the regenerative chatter is supposed to occur is 3906 [Hz], and the corresponding dynamic compliance is -3.141 [μm/N]. Note that the cross components of the dynamic compliance G_{xy} and G_{yx} are approximately equal to zero, which matches the supposition when deriving Eq. (3). Figure 13 shows the dynamic compliance of a 4-tooth 45 deg/44 deg ordinarily-varied-helix end mill (No. 2) fixed to the spindle at a projection length of 41 [mm]. The negative peak frequency is 3437 [Hz] and the corresponding dynamic compliance is -4.273 [μm/N]. For convenience, only the direct component of the radial depth of cut direction is shown for the dynamic compliances for the projection lengths of 41 and 46 [mm]. Note that the cross components of the dynamic compliances for the varied-helix end mills were measured also and confirmed that they are similar to the standard end mill, and therefore their cross components are also assumed as zero. Figure 14 shows the dynamic compliance of a 4-tooth standard end mill (No. 1) set to a projection length of 46 [mm]. The negative peak frequency is 2627 [Hz], and the dynamic compliance is -8.036 [μm/N].
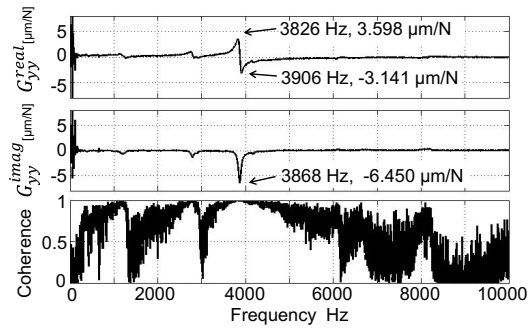
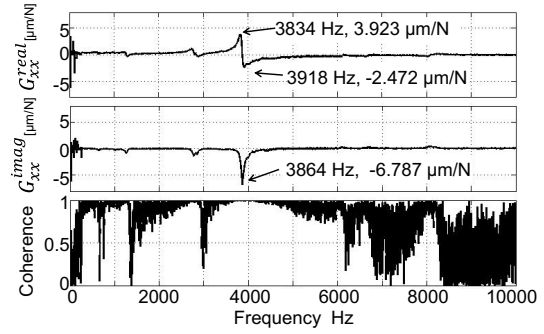(a) Dynamic compliance in *y* direction
   by *y* direction impulse.
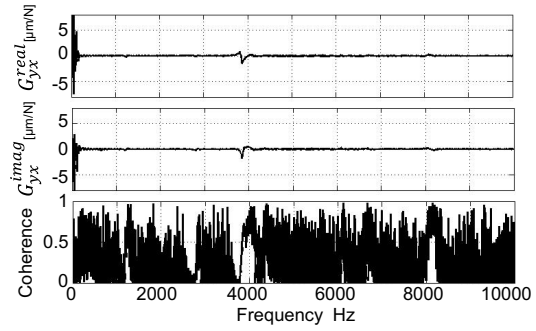
(b) Dynamic compliance in *y* direction
   by *x* direction impulse.
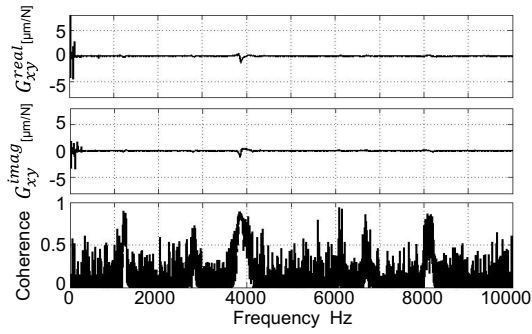
(c) Dynamic compliance of *x* direction
   by *y* direction impulse.

(d) Dynamic compliance of *x* direction
   by *x* direction impulse.

Fig. 12. Measured dynamic compliances of 4-flute standard helix end mill (No.1) fixed at projection length of 36 [mm] in the feed (x) and radial depth of cut (y) direction after milling test.
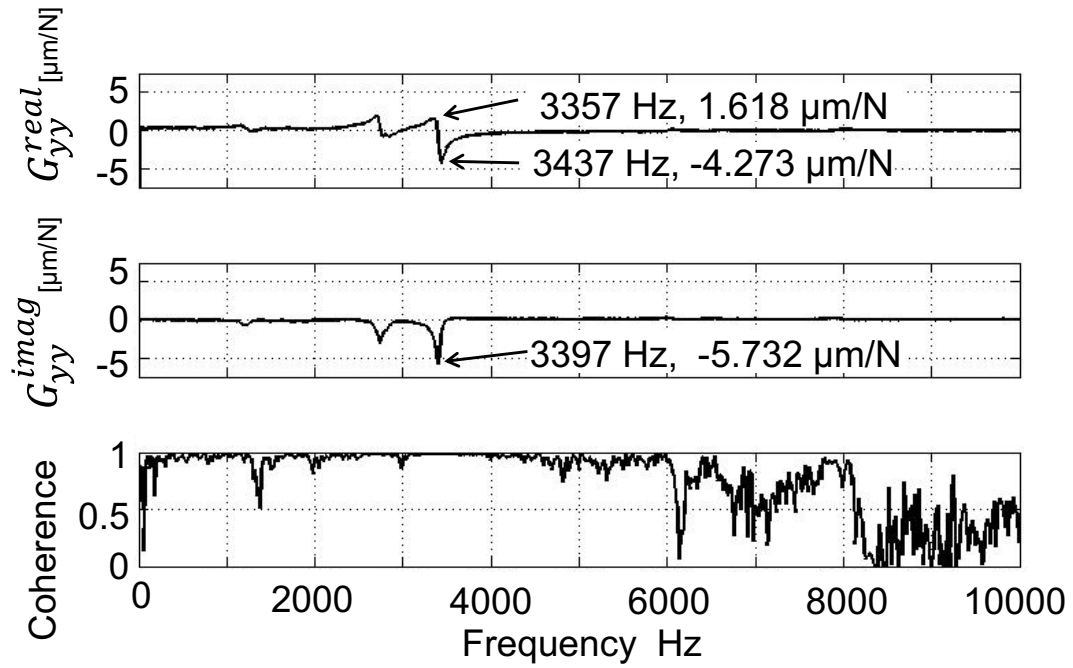
Fig. 13. Measured dynamic compliance of 4-flute 45 deg/44 deg ordinarily-varied-helix end mill (No.2) fixed at projection length of 41 [mm].
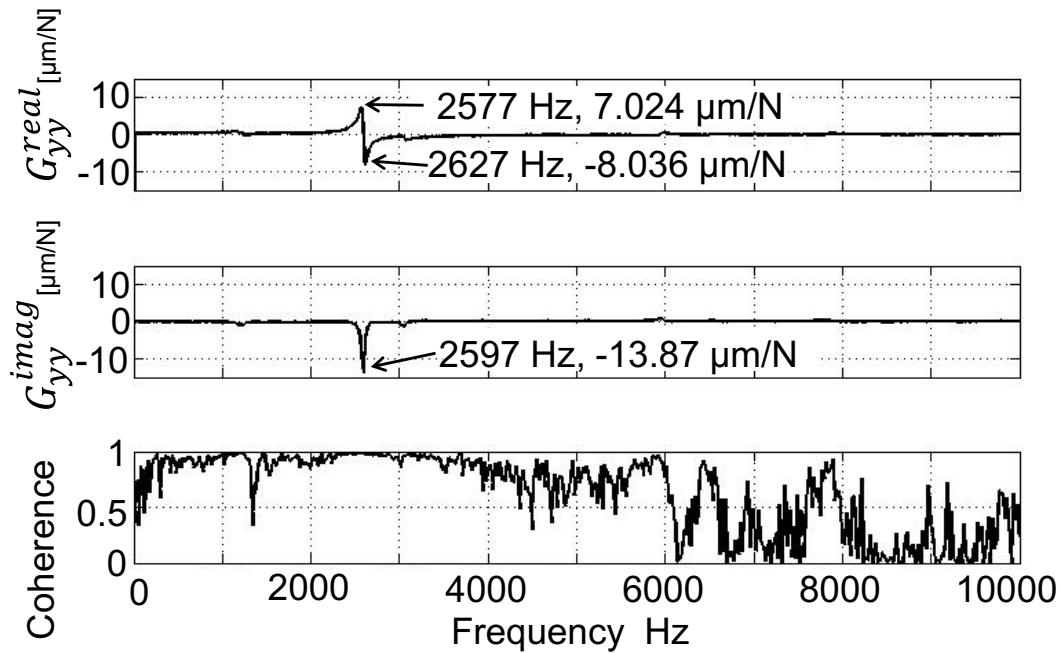
Fig. 14. Measured dynamic compliance of 4-flute standard end mill (No.1) fixed at projection length of 46 [mm].

Through these impulse hammer tests, it is confirmed that the negative peak frequency and the dynamic compliance of a 4-tooth standard end mill (No. 1), 45 deg/44 deg ordinarily-varied-helix end mill (No. 2), and 45 deg/40 deg highly-varied-helix end mill (No. 3) are almost equal to each other. From these results, it is reasonable that the longer the projection of an end mill, the

lower the negative peak frequency and higher the dynamic compliance.

4.4 Comparison of radial cutting force between workpieces

In machining with extremely small radial immersion, work hardening causes the workpiece to harden, and thus the radial cutting force is not linear to the original hardness of the workpiece. Therefore, milling experiments were carried out to determine the radial cutting force when machining 60 HRC and 15 HRC steels. The cutting conditions are the same as shown in Table 2. The cutting force in peripheral milling with the 45 deg/40 deg highly-varied-helix end mill (No. 3) is measured at a relatively low spindle speed since the cutting force is stable and chatter-less.

Table 5 shows the cutting forces F_{60} and F_{15} in the radial depth of cut direction when machining 60 HRC and 15 HRC steels respectively. 60 HRC steel was machined with the end mill set at the projection length of 36 [mm], while 15 HRC steel was machined at 41 [mm]. For example, the measured cutting forces of 60 HRC and 15 HRC steels at a spindle speed of 3000 [min^{-1}] are shown in Figs. 15 and 16 respectively. From these figures, the maximum and minimum of the cutting forces during one rotation of the spindle is calculated considering the whirling of the teeth of the end mill. The average cutting force was calculated from one million data points in 4 different spindle speeds as shown in Table 5, and they were averaged to obtain the ratio of radial cutting force $\frac{F_{15}}{F_{60}} = 0.573$.

Table 5
Comparison of radial cutting forces in machining 60 and 15 HRC steels

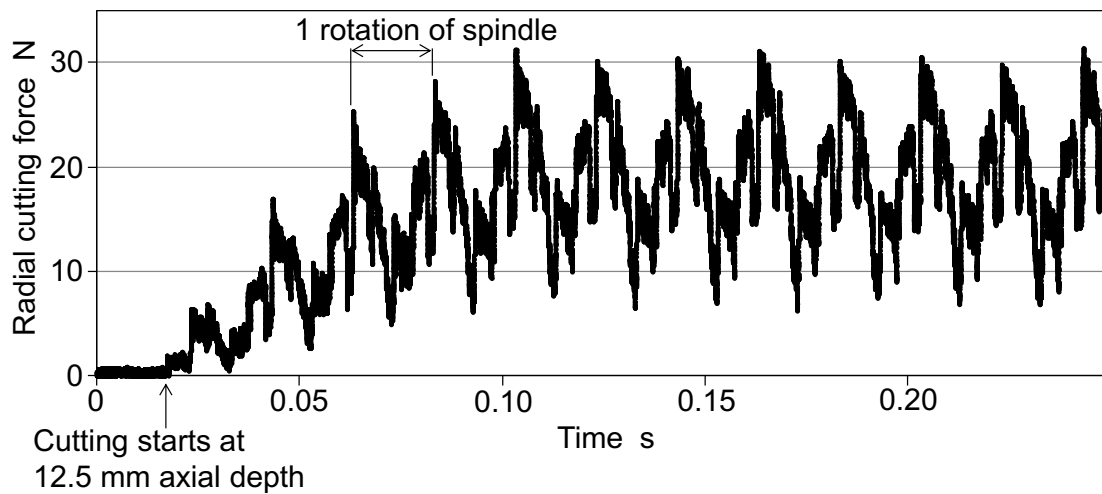| Spindle speed n [min^{-1}]	Average normal cutting force		
	60 HRC steel	15 HRC steel	F_{15}/F_{60}
	F_{60} [N]	F_{15} [N]	
2500	16.871	9.927	0.588
3000	16.532	9.614	0.582
3500	15.626	8.913	0.570
4000	16.570	9.162	0.553
Average	16.400	9.404	0.573

Fig. 15. Cutting force in radial depth of cut direction of 60 HRC steel with 45 deg/40 deg highly-varied-helix end mill (No.3) at projection length of 36 [mm] and spindle speed of 3000 [min^{-1}].
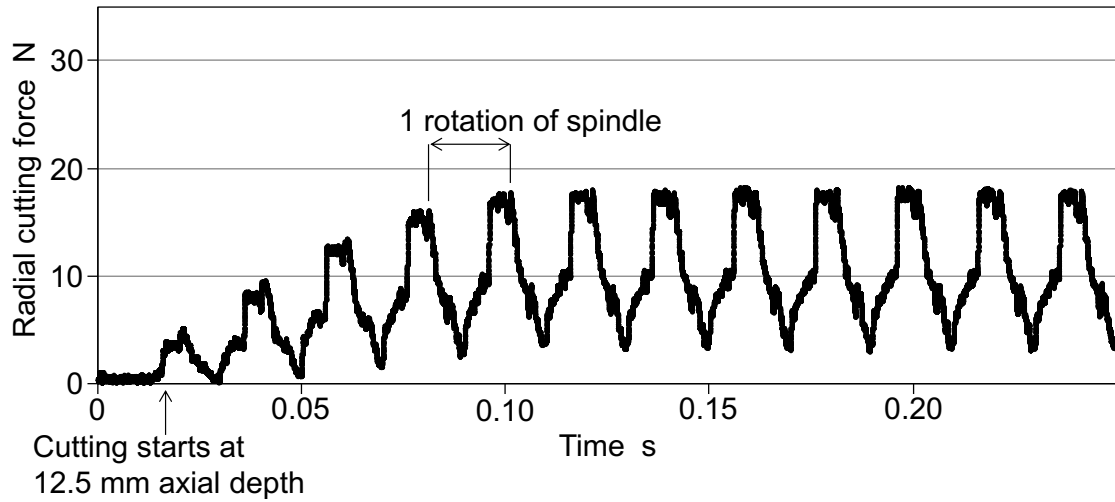
Fig. 16. Cutting force in radial depth of cut direction of 15 HRC steel with 45 deg/40 deg highly-varied-helix end mill (No.3) at projection length of 41 [mm] and spindle speed of 3000 [min^{-1}].

4.5 Experimental results and discussions

Experiments were conducted under the conditions shown in Table 2. Examples of the machined surfaces of the larger workpiece are shown in Figs. 17 - 22. Figures 17 and 18 are the surfaces machined by the standard end mill (No. 1) at projection lengths of 36 and 41 [mm] at the spindle speed of 7000 [min^{-1}]. Severe chatter can be observed in these surfaces. Figure 19 is the surface machined by the 45 deg/44 deg ordinarily-varied-helix end mill (No. 2) at projection length of 41 [mm] at the spindle speed of 7000 [min^{-1}]. This matches well with the predicted result from the value of the proposed design index $\frac{a_p}{a_{\lim}}$ as shown in Table 4. Figures 20 and 21 are the surfaces machined by the 45 deg/40 deg highly-varied-helix end mill (No. 3) at projection lengths of 36 and 41 [mm] at the spindle speed of 7000 [min^{-1}]. It can be observed that they are chatter-free surfaces. This also matches the predicted result from the value of the proposed design index as shown in Table 4, which verifies that the proposed index can be used effectively to perform chatter-free machining with the designed varied-helix end mills. This can also be confirmed in the machined surface by the 45 deg/40 deg highly-varied-helix end mill (No. 3) at projection length of 46 [mm] at the spindle speed of 7000 min^{-1} shown in Fig. 22, where surfaces at conditions in high axial depths of cut result in chatter vibration, which matches well with the value of the proposed design index shown in Table 4.
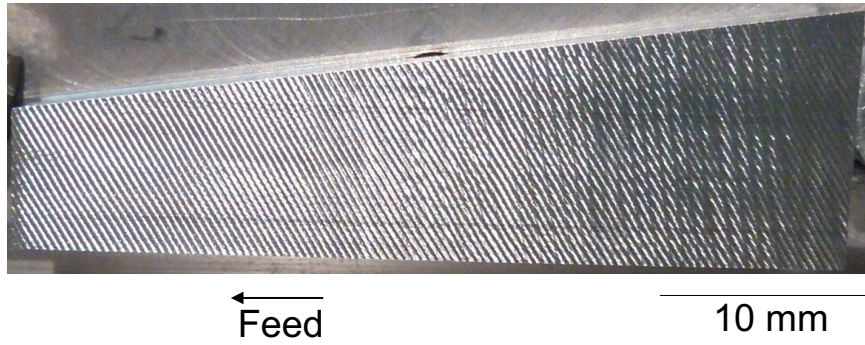
Fig. 17. Surface of 60 HRC steel machined with chatter by using 4-flute standard end mill (No.1) at projection length of 36 [mm] and spindle speed of 7000 [min^{-1}].
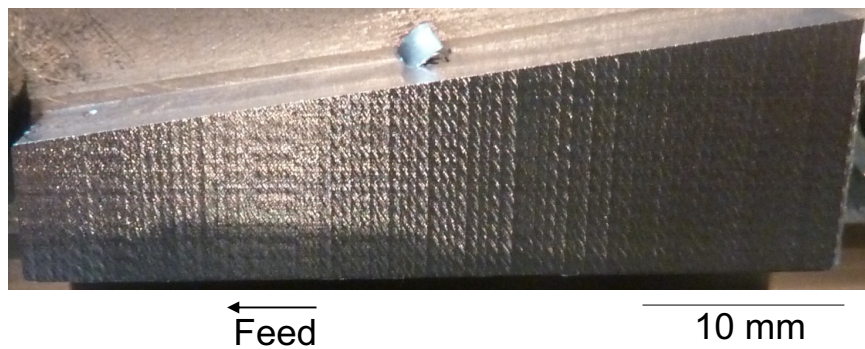

Fig. 18. Surface of 15 HRC steel machined with chatter by using 4-flute standard end mill (No.1) at projection length of 41 [mm] and spindle speed of 7000 [min^{-1}].
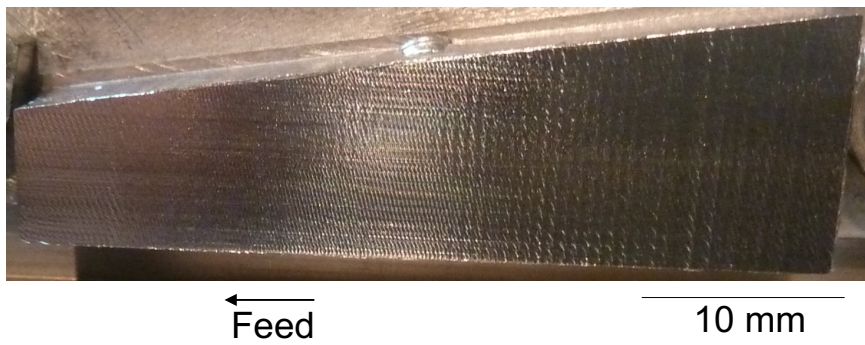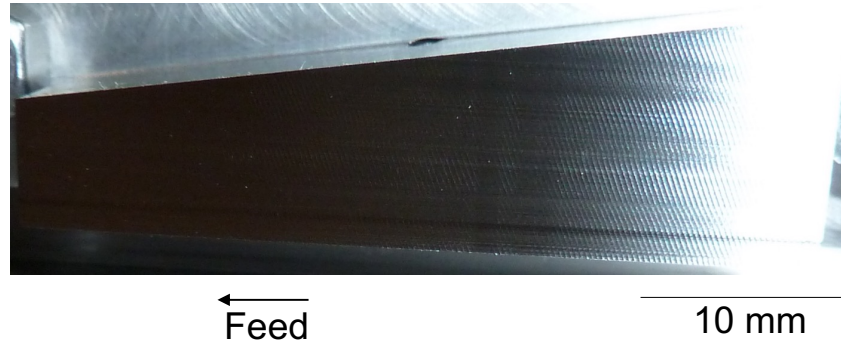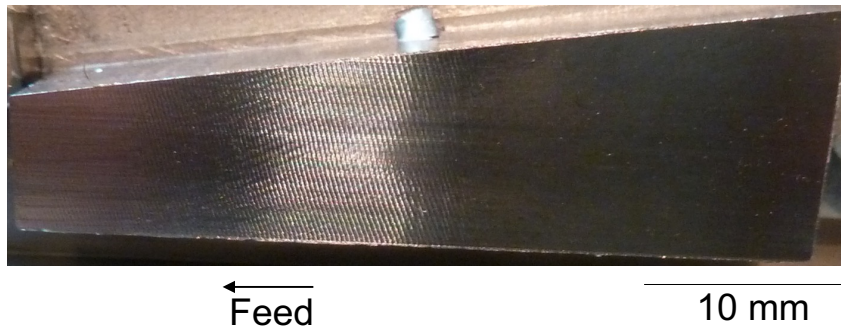

Fig. 19. Surface of 15 HRC steel machined with and without chatter by using 4-flute 45 deg/44 deg ordinarily-varied-helix end mill (No.2) at projection length of 41 [mm] and spindle speed of 7000 [min^{-1}].
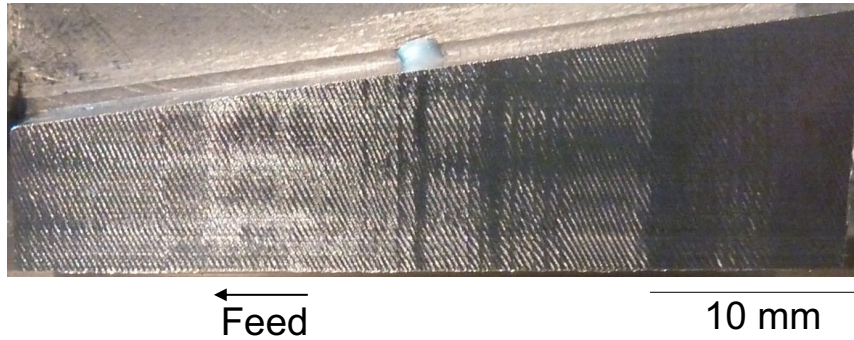
Feed   10 mm

Fig. 20. Surface of 60 HRC steel machined without chatter by using 4-flute 45 deg/44 deg highly-varied-helix end mill (No.3) at projection length of 36 [mm] and spindle speed of 7000 [min^{-1}].

Feed   10 mm

Fig. 21. Surface of 15 HRC steel machined without chatter by using 4-flute 45 deg/40 deg highly-varied-helix end mill (No.3) at projection length of 41 [mm] and spindle speed of 7000 [min^{-1}].

Feed   10 mm

Fig. 22. Surface of 15 HRC steel machined with and without chatter by using 4-flute 45 deg/40 deg highly-varied-helix end mill (No.3) at projection length of 46 [mm] and spindle speed of 7000 [min^{-1}].

Figures 23 - 29 show the overall results of the peripheral milling with the three types of 4-tooth end mills. The results of projection lengths of 36 and 41 [mm] of the standard end mill (No. 1) are shown in Figs. 23 and 24 respectively. The marks "○", "△", "×" are classified by the measured vibration peaks a_c near the negative peak frequency of the real part of the dynamic compliance, which corresponds to the frequency of the chatter vibration, and they represent $a_c \leq$ 1μm, 1μm$\leq a_c \leq$ 2μm, and $a_c \geq$ 2μm respectively. In Figs. 23 and 24, it can be observed that although the results in low spindle speed tend to be stable, it is confirmed that unstable cutting is

performed throughout a wide region. Moreover, the stable region in the low spindle speed is thought to happen because of process damping [16], since the cutting speed at for example 2500 [min^{-1}] is 62.83 [m/min]. In addition, even at the worst conditions where a_{lim} is smallest, they tend to be greater than the theoretical value calculated by Eq. (6) which are 1.41 and 1.81 [mm] for Figs. 23 and 24 respectively. This is thought to happen because of the swing of the end mill clamped to the tool holder, which results in unbalanced cutting by the teeth tending to result in more stable cutting.
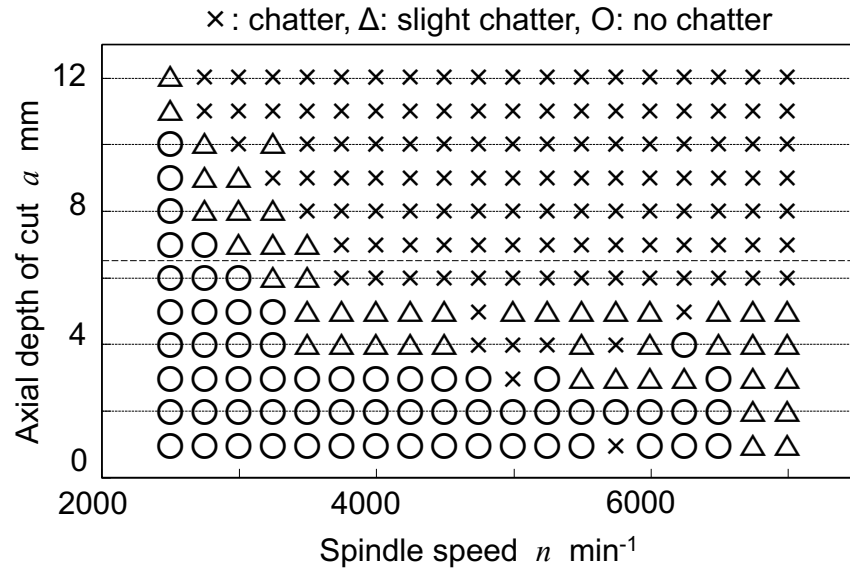
Fig. 23. Results of milling 60 HRC steel at projection length of 36 [mm] with standard end mill (No.1).
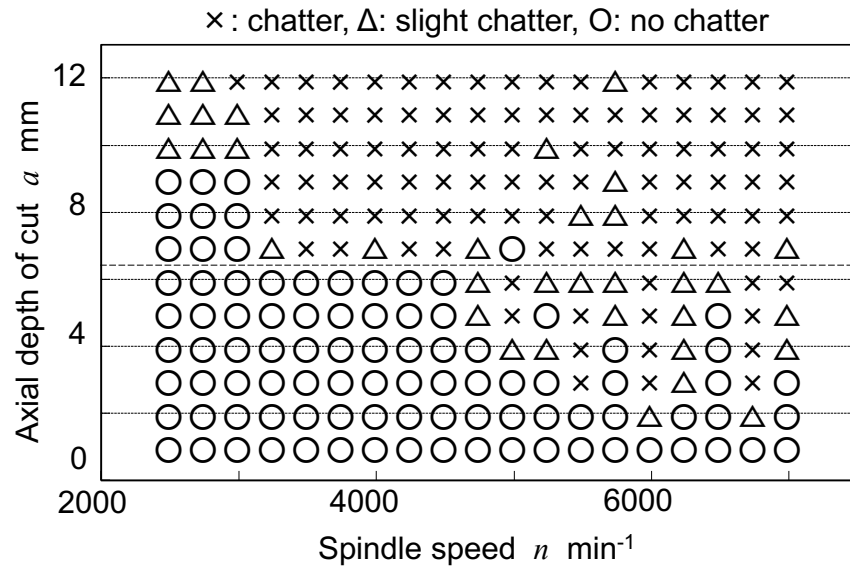

Fig. 24. Results of milling 15 HRC steel at projection length of 41 [mm] with standard end mill (No.1).

Figures 25 and 26 show the results of projection lengths of 36 and 41 [mm] of the 45 deg/44

deg ordinarily-varied-helix end mill (No. 2) respectively. The black solid lines in the figures represent the cancellation lines of regenerative chatter. From these results, it can be observed that there are unstable regions throughout all conditions. This can be explained by the proposed design index, since the values of them in all conditions are less than the threshold value. Note that not all conditions near the regenerative effect cancellation lines are chatter-free. This is because the cancellation lines are calculated only by the negative peak frequency of the real part of the dynamic compliance, therefore meaning that they are not effective for other frequencies. As a result, chatter vibration occurs at higher frequencies than expected. As mentioned earlier, this is why it is important to satisfy the proposed threshold value since it covers for these cases also.
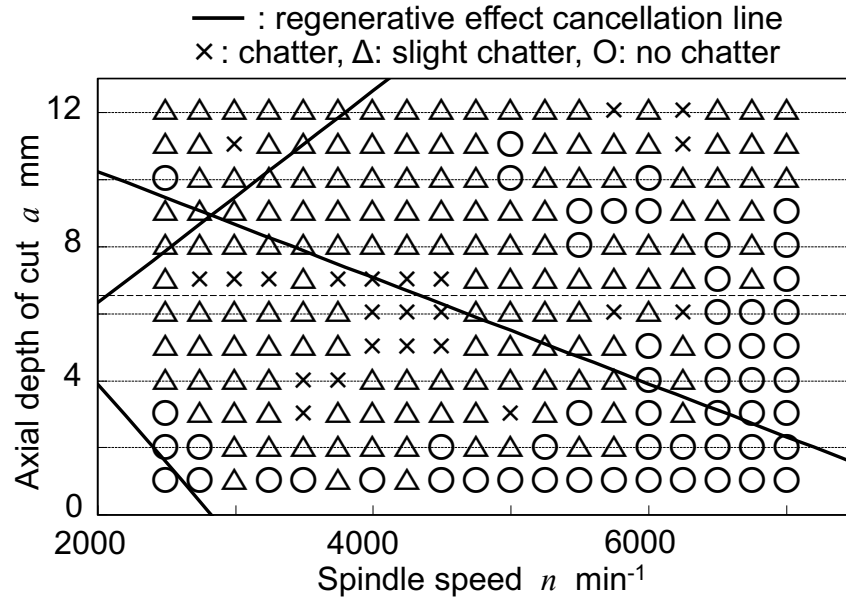
Fig. 25. Results of milling 60 HRC steel at projection length of 36 [mm] with 45 deg/44 deg ordinarily-varied-helix end mill (No.2).
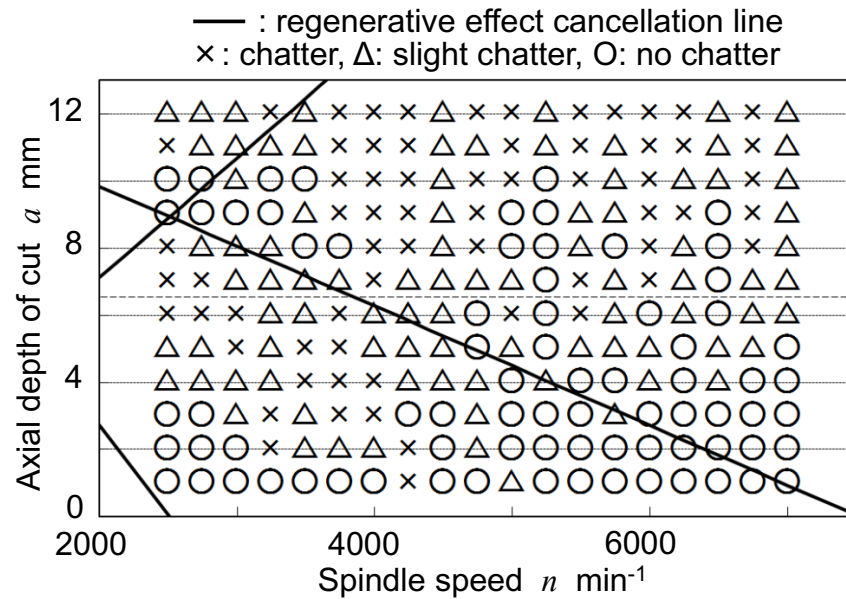
Fig. 26. Results of milling 15 HRC steel at projection length of 41 [mm] with 45 deg/44 deg ordinarily-varied-helix end mill (No.2)

Figures 27, 28, and 29 show the results of projection lengths of 36, 41, and 46 [mm] of the 45 deg/40 deg highly-varied-helix end mill (No. 3) respectively. In Figs. 27 and 28, it can be observed that almost all conditions are chatter-free, which proves the effectiveness of the highly-varied-helix end mill designed by the proposed design index. On the other hand, it can also be observed in Fig. 29 that some conditions are unstable. This is understood by the fact that $\frac{a_p}{a_{\lim}}$ is greater than the threshold value in those conditions, and it is reasonable.
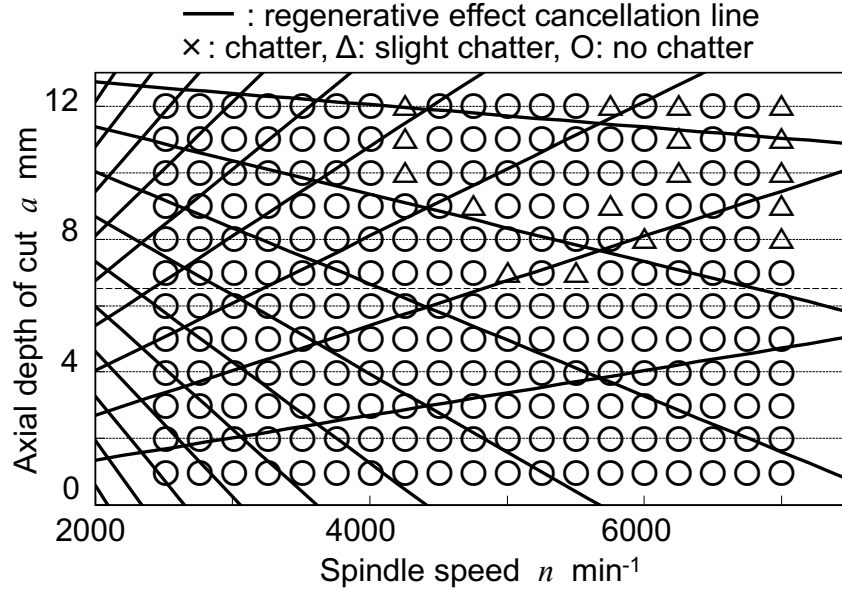

Fig. 27. Results of milling 60 HRC steel at projection length of 36 [mm] with 45 deg/40 deg highly-varied-helix end mill (No.3).
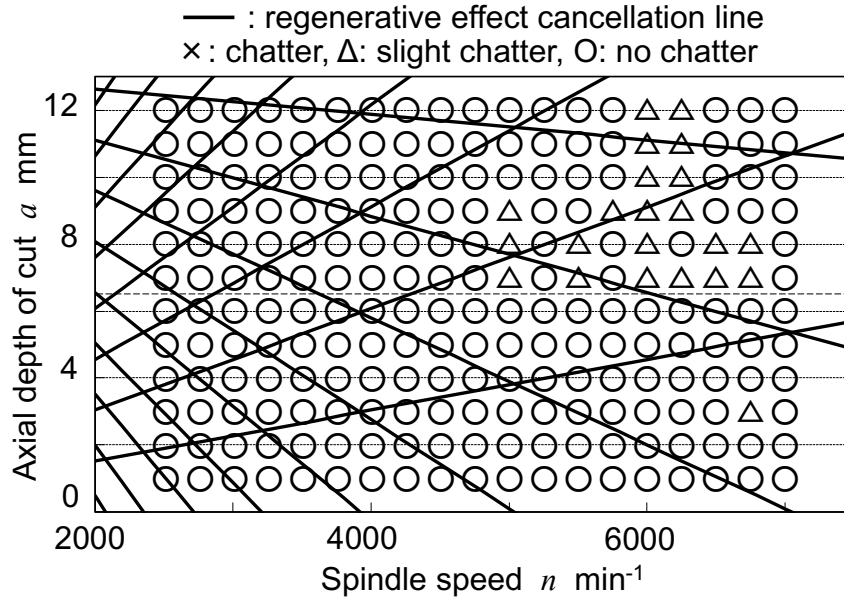

Fig. 28. Results of milling 15 HRC steel at projection length of 41 [mm] with 45 deg/40 deg highly-varied-helix end mill (No.3).
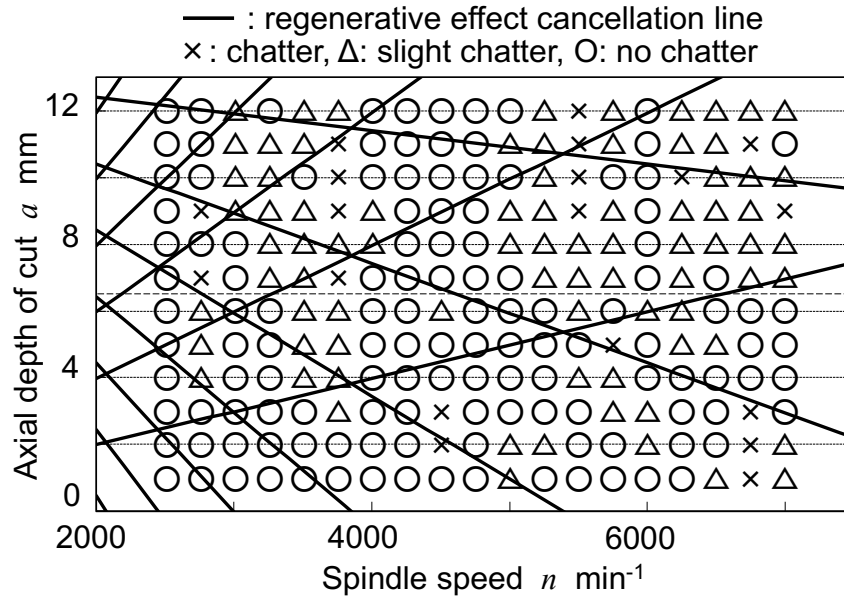
Fig. 29. Results of milling 15 HRC steel at projection length of 46 [mm] with 45 deg/40 deg highly-varied-helix end mill (No.3).

In summary, the above experimental results show that the proposed design index $\frac{a_p}{a_{\lim}}$ can be used effectively to design varied-helix end mills. Using these end mills, high-efficiency peripheral milling of hardened steel can be realized successfully, with both mode coupling and regenerative chatter vibrations suppressed.

5 Conclusion

Peripheral milling with small radial immersion was considered in the present paper. According to some simplifications, the asymptotic chatter stability limit was determined for the process, and it was shown that it is similar to that of plunge turning. In this particular cutting process, both mode coupling chatter and regenerative chatter need to be suppressed for stable cutting. According to an analytical simulation, it was shown that there is a critical immersion angle and as long as cutting is performed below this angle, mode coupling chatter can be suppressed. In addition, the mechanism of suppression of regenerative chatter by varied-helix end mills was explained utilizing the regenerative effect cancellation diagram. Based on the mechanism of varied-helix end mills, a design index $\frac{a_p}{a_{\lim}}$ was proposed for robust chatter-free designs of varied-helix end mills, and its threshold value was obtained theoretically. The validity of the proposed index and threshold value was verified through a series of simulations and experiments, and it was confirmed that the proposed design index can be used effectively to suppress regenerative chatter vibration. Not only is the proposed index able to be used for peripheral milling of hardened materials with extremely small radial immersion, but it can also be used in a variety of processes which implies that the proposed index is a universal one.

Acknowledgements

References

[1] Ito A, Suzuki N, Shamoto E. Suppression of regenerative chatter vibration in peripheral finishing of hardened steel with variable helix end mills. 7th International Conference and Exhibition on Design and Production of Machines and Dies/Molds 2013;123-128.

[2] Ito A, Shamoto E. An innovative machining strategy for efficient peripheral finishing of hard materials with highly-varied-helix end mill. International Journal of Automation Technology 2015;9(2):153-160.

[3] Ito A, Shamoto E. Proposal of low-radial and high-axial immersion machining of hard materials with highly-varied-helix end mill. Journal of the Japan Society Precision Engineering 2015; 81(9): 867-874.

[4] Altintas Y, Stepan G, Merdol G, Dombovari Z. Chatter stability of milling in frequency and discrete time domain. CIRP Journal of Manufacturing Science and Technology 2008;1:35-44.

[5] Altintas Y, Budak E. Analytical prediction of stability lobes in milling. Annals of CIRP 1995;44(1):357-362.

[6] Altintas Y, Shamoto E, Lee P, Budak E. Analytical prediction of stability lobes in ball end milling, Transactions of ASME Jounal of Manufactuing Science and Engineering 1999;121:586-592.

[7] Budak E, Altintas Y. Analytical prediction of chatter stability in milling-Part I: General foumulation. Transactions of ASME Journal of Dynamic Systems Measurement and Control 1998;120(1):22-30.

[8] Budak E, Altintas Y. Analytical prediction of chatter stability in milling-Part II: Application of the general formulation to common milling systems. Transactions of ASME Journal of Dynamic Systems Measurement and Control 1998;120(1):31-36.

[9] Merdol S.D, Atlintas Y. Multi frequency solution of chatter stability for low immersion milling. Transactions of ASME Jounal of Manufactuing Science and Engineering 2004;126:459-466.

[10] Altintas Y, Engin S, Budak E. Analytical stability prediction and design of variable pitch cutters. Transactions of ASME Journal of Manufacturing Science and Engineering 1999;121(1):173-178.

[11] Budak E. An analytical design method for milling cutters with non-constant pitch to increase stability, Part 1: Theory. ASME Journal of Manufacturing Science and Engineering 2003;125(2):29-34.

[12] Budak E. An analytical design method for milling cutters with non-constant pitch to increase stability, Part 2: Application. ASME Journal of Manufacturing Science and Engineering 2003;125(2):35-38.

[13] Sims N.D, Mann B, Huyanan S. Analytical prediction of chatter stability for variable pitch and variable helix milling tools. Journal of Sound and Vibration 2008;317,Issues 3-5:664-686.

[14] Altintas Y. Manufacturing Automation. Cambridge University Press;2012:149-154.

[15] Insperger T, Munoa J, Zatarain M, Peigne G. Unstable Islands in the Stability Chart of Milling Processes Due to the Helix Angle. CIRP 2nd International Conference on High Performance Cutting 2006. 12-13.

[16]   Altintas Y, Eynian M, Onozuka H. Identification of dynamic cutting force coefficients and chatter stability with process damping. Annals of CIRP 2008;57(1):371-374.